ISBN: 978-3-95450-234-9 ISSN: 2673-5504 doi:10.18429/JACoW-SRF2023-MOPMB041

MICROSTRUCTURE DEVELOPMENT IN A COLD WORKED SRF NIOBIUM SHEET AFTER HEAT TREATMENTS*

S. Balachandran[1,†], P. Dhakal[1], S. Chetri[2], P. J. Lee[2], Z. Thune[3], T. R. Bieler[3], A. M. Valente-Feliciano[1]
[1]Thomas Jefferson National Accelerator Facility, Newport News, VA, USA
[2]National High Magnetic Field Laboratory, ASC, FSU, Tallahassee, FL, USA
[3]Department of Chemical Engineering and Material Science, MSU, East Lansing, MI, USA

Abstract

Bulk Nb for TESLA shaped SRF cavities is a mature technology, with high gradient (>35 MV/m) and high Q_0 cavities (10^{9-10},T= 2 K) routinely fabricated. Significant advances are necessary to push Q_0's to 10^{10-11}(T= 2 K), and involve modifications to the sub-surface Nb layers by impurity doping. In order to achieve the lowest surface resistance any trapped flux needs to be expelled for cavities to reach high Q_0's. There is clear evidence that cavities fabricated from polycrystalline sheets meeting current specifications require higher temperatures beyond 800 °C for better flux expulsion. Recently, cavities fabricated with a non-traditional Nb sheet with initial cold work due to cold rolling expelled flux better after 800 °C/3 h heat treatment than cavities fabricated using fine-grain polycrystalline Nb sheets. Here, we analyze the microstructural development of Nb from the vendor supplied cold work non-annealed sheet that was fabricated into an SRF cavity as a function of heat treatment building upon the methodology development to analyze microstructure being developed by the FSU-MSU-UT, Austin-JLAB collaboration. The results indicate correlation between full recrystallization and better flux expulsion.

INTRODUCTION

Superconducting radio frequency (SRF) Nb cavities have been the workhorse for delivering high-quality, high energy beams for high-energy physics, nuclear physics, and microscopy applications [1]. The main driver for current Nb cavity technology is to decrease the footprint by pushing towards the maximum possible gradients and high efficiency defined by high quality factor ($Q_0 > 10^{10}$, T=2 K) [2]. Interstitial additions through surface diffusion of N [3,4], O [5–7] have shown that carefully tuning the surface layers leads to high Q_0's, presently in the gradient range of 10-20 MV/m. The pursuit of high Q_0 has led to uncovering the influence of trapped flux on the surface resistance which scales linearly in the range of 1-2 nΩ/mG [8,9] in Nb cavities thus limiting the highest Q_0 attainable. It is widely accepted that the trapped flux, and flux expulsion is a bulk phenomena and dominated by bulk Nb microstructure [10, 11], whereas surface modifications increase the propensity to trap flux [12, 13]. Work around to improve flux expulsion have typically involved increase in final heat treatment temperatures in the range of 900-1000 °C [14] and faster cool-down by using a higher temperature differential through the superconducting transition of Nb (T_c= 9.2 K) [15].

Improved flux expulsion with increase in heat treatment temperature has led us to the following driving questions: Would an improved recrystallized microstructure lead to better flux expulsion? Can we promote full recrystallization by adopting a newer fabrication strategy of starting with a cold-worked sheet and fabricating a cavity and then performing an 800 °C/3 h heat treatment? Our preliminary results indicate that a sheet with initial cold work can be fabricated into an SRF Nb cavity, and heat treatment at 800 °C/3 h shows a much improved flux expulsion performance than a traditionally fabricated SRF Nb cavity as shown in Fig. 1 [16] [and this conference]. In a traditionally fabricated Nb cavity with fine grain size sheet or large grain Nb, surface damage, strain path and location in SRF Nb cavities have an influence on recrystallization and temperatures as high as 1000 °C may not be sufficient to remove all defects contributing to flux trapping [17,18]. Hence, changes in processing path applied to SRF Nb sheets fabricated into cavities need to be evaluated in terms of microstructure development with respect to heat treatments.

In the following paper we track the microstructure development in the cold work/non-annealed (NA) sheet as supplied from Vendor A, that was used to make the cavity that expels flux better than a standard cavity even after 800 °C/3 h. To track the recrystallization behavior we use cross-sectional micro-texture data collected from heat treated SRF Nb sheet at 700 °C/3 h - 900 °C/3 h and extend the approach of determining recrystallization through the analysis of geometrically necessary dislocations (GND) that is being currently developed for Nb [19, 20]. Our results indicate high levels of recrystallization at 800 °C/3 h in the sheet that was used in the fabrication of the better flux expelling SRF Nb cavity.

MATERIALS AND METHODS

The starting material is the as-received sheet from an SRF Nb supplier, Vendor A, with unknown percent cold work and no heat treatments. Since the sheet was requested in an off-specification condition (without a final anneal), the residual resistivity ratio (RRR), hardness and mechanical strength is not certified. However, the initial composition

* Work supported by U.S. DOE, Office of Science, Office of HEP under Award No. DE-SC0009960. NHMFL- NSF Cooperative Agreement No. NSF DMR-1644779 (-2022) DMR-2128556 (2023-), the State of Florida, and JSA, LLC U.S. DOE Contract No. DE-AC05- 06OR23177.
† shreyas@jlab.org

ISBN: 978-3-95450-234-9 ISSN: 2673-5504 doi:10.18429/JACoW-SRF2023-MOPMB041

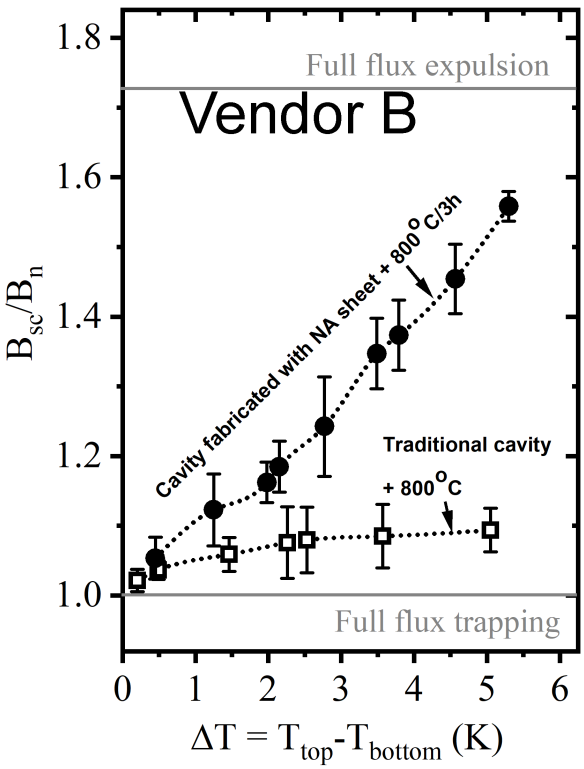

Figure 1: Flux expulsion behavior of two cavities after a 800 °C/3 h heat treatment fabricated from Nb sheets supplied by an SRF qualified Nb vendor B. A traditional cavity adopts a fine grain polycrystalline Nb sheet. The cavity that expels flux better is fabricated with a cold work, non-annealed sheet with an initial deformed microstructure.

of the metal and interstitial content (O, H, C, N) meet the current SRF polycrystalline Nb sheet specification.

Heat Treatments on Coupon Samples

Three-hour heat treatments at 300 °C, 500 °C, 600 °C, 700 °C, and 900 °C, were performed on 3 mm × 3 mm × 10 mm samples sealed in an evacuated quartz tube and back filled with ultrahigh purity Argon (Airgas- AR-UHP 300) to a pressure of 400 mTorr, in a three-zone tube furnace with a uniform hot zone of 100 mm. A Type K thermocouple was placed adjacent to the sample in a quartz tube to record the temperature. The furnace was ramped from room temperature to 50 °C in 30 minutes and held at 50 °C for 30 minutes before ramping to the heat treatments temperature at 5 °C/min. The temperature profile from the thermocouple corresponds with the set ramp rate. The final temperature (T_f) was within ± 3 °C of the set temperature, there was an initial overshoot of 22 °C for the 700 °C heat treated sample, but the temperature stabilized in 15 minutes to T_f = 700 °C. Soak times for all samples at T_f were three hours. The samples were furnace-cooled. Heat treatments at 800 °C, and 900 °C were performed in the JLAB cavity heat treatment furnace.

Sample Preparation for Microscopy

The samples were hot mounted in a Conductomet ® to form a 25 mm puck. Sample preparation involved successive grinding and polishing steps with SiC abrasive with grit sizes of 320, 400, 600, 800, and 1000, and subsequently with a non-water based 5 µm, 3 µm , and 1 µm diamond suspension. An automatic polisher (Allied) with an 8 inch wheel was used for planarization and polishing of the samples. The polishing load per sample was 4 lbs for SiC grits and dropped to 3 lbs for diamond suspensions. The polishing times were 60 s for SiC grits and 240 s for diamond polishing. The final polishing to achieve a damage free surface was performed in a vibratory polisher (Buehler Vibromet II ®), using a 50 nm colloidal silica solution (Buehler Mastermet®) with ph of 11.5. The samples were initially polished for ~24 h and then lightly buffer chemically polished with a 1:1:2 ($HF : HNO_3 : H_3PO_4$) solution for 60 seconds and final polishing was continued for another 24-48 h in the Vibromet to obtain damage free surfaces.

Details of Electron Backscatter Diffraction (EBSD) Microscopy and Calculation of GND Density

The EBSD setup involves, the EDAX Velocity® camera with the capability of greater than 2000 indexed points per second, and angular precision below 0.1° in a LaB6 filament, Tescan Vega 3 microscope. Data analysis was performed using the EDAX-TSL-OIM software version 8.5.1002. A step size for 1 µm, 1 x 1 binning, and a scan area of 500 µm x 500 µm was used to generate the data for the software to calculate the geometrically necessary dislocation (GND) density using a gradient methodology [21]. The maximum misorientation considered is 5°, the Burgers vector (b) magnitude is 0.28665 nm, and the nearest neighbor is one. All three families of slip systems- {110}<111>, {112}<111>, and {123}<111> for Nb are considered.

RESULTS

Microstructure Development in Non-Annealed Sheet with Heat Treatment

In Fig. 2, EBSD-generated maps of the cross-sectional samples show the evolution of the Nb microstructure within 600 µm of the top surface (labeled "top"): The IPF maps (a-d) provide the micro-texture orientation information needed to calculate GND density, while the corresponding IQ maps (e-f) provide a microstructure visualization with the contrast indicating topography, surface quality, strain, and grain boundaries [22].

Figure 2a, shows the high level of rolling deformation retained in the non-annealed (NA) starting sheet used to make the cavity, and the corresponding IQ map in Fig. 2e, indicates the associated strain contrast. After a 700 °C/3 h heat, the NA microstructure is partially recrystallized with the development of discernible grain size in the order of tens of µm as observed in Fig. 2b. However, there are

ISBN: 978-3-95450-234-9 ISSN: 2673-5504 doi:10.18429/JACoW-SRF2023-MOPMB041

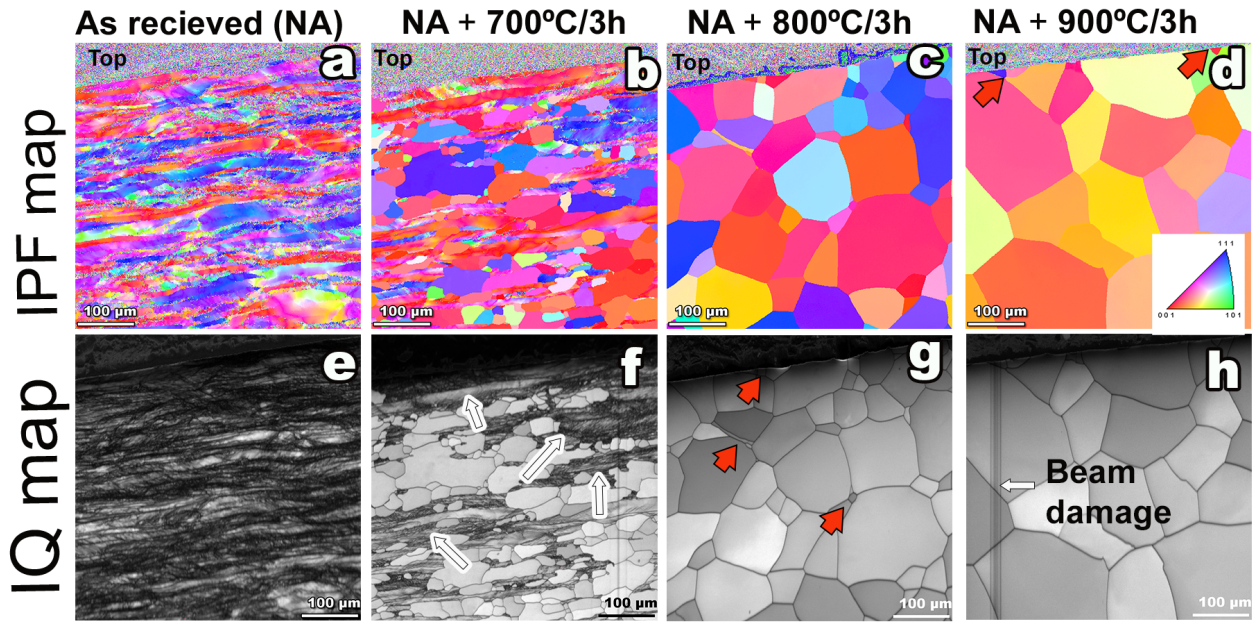

Figure 2: Crossectional EBSD images in the as received state and after 3 h heat treatments. The inverse pole figure (IPF) on the top row and the corresponsding image quality (IQ) map on the bottom row for (a,e) non-annealed, as received, (b, f) after 700 °C/3 h, (c, g) 800 °C/3 h, and (d, h) 900 °C/3 h. Note the growth in the grain size and improvement in the image quality (IQ) with increased heat treatment temperature. Also, notice the fine grains indicated by arrows after 800 °C/3 h (g), and 900 °C/3 h.

regions within this microstructure that are not recrystallized, as indicated by the dark regions in the IQ map in Fig. 2. IPF's in Fig. 2c, d, reveal significant grain growth after 800 °C, and 900 °C and the corresponding IQ maps in Fig. 2g,h, do not indicate any intragrain strain contrast. Qualitatively speaking the observations of the IQ map suggest that full recrystallization and grain growth occur after 800 °C/3 h. There are also fine grains that seem trapped between larger grains after 800 °C/3 h (Fig. 2g), and at the surface after 900 °C/3 h (Fig. 2h). There is the suggestion of a grain size gradient from the top surface in the 800 °C. However, a more prominent grain counts, and an analysis based on the thickness needs to be performed to determine if the observation is significant.

In order to quantify the observations in Fig. 2, we have plotted the average IQ and grain size as a function of temperature in Fig. 3. The average IQ scales with the heat treatment temperature, with the lowest average IQ of ~9000 occurring in the NA starting sheet, whereas the highest average IQ of ~29000 appears in the 800 °C/3 h map, with the 700 °C/3 h sample showing an intermediate average IQ of 25000, which is between the extremes values. The slightly lower average value of the IQ map after 900 °C/3 h is surprising and may be due to beam damage (carbon deposition during previous scan suspected) that is observed in the IQ map in Fig 2h. If we were to predict the recrystallization percent in the 700 °C/3 h sample from the average values of the IQ map using the formula: [IQ(700 °C/3 h)- IQ(NA)]/ [IQ(800 °C/3 h)-IQ(NA)], we have a recrystallized percentage of 70 %.

The average grain size after three-hour heat treatments at 700 °C, 800 °C, and 900 °C are 51 ± 2 µm, 141 ± 6 µm, and 211 ± 13 µm. The grain size averages are obtained from 1500 µm x 1500 µm area scans and not presented in this paper. The small grains observed in the 800 °C/3 h maps have an average value of 32 ± 4 µm, which is ~23% of the average grain size. The smaller grains in the 900 °C sample have an average value of 62 ± 4 µm, which is 44% of the average grain size. The presence of these fine grains in the cross sectional images of the recrystallized matrix after 800 °C, and 900 °C, may be important.

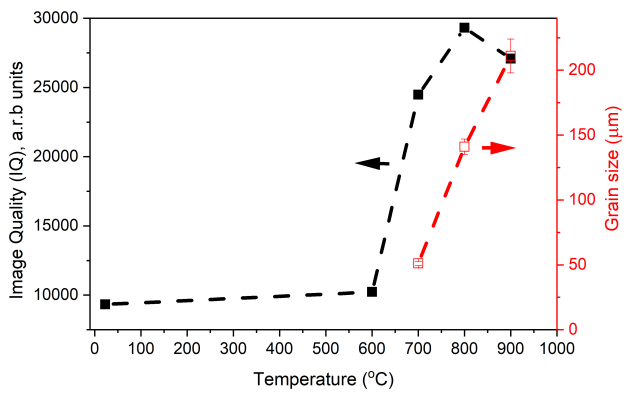

Figure 3: Average image quality (IQ) numbers and grain size evolution as a function of heat treatment temperature. The average IQ index improves with heat treatment. The grain size is linearly correlated with heat treatment temperatures of 700-900 °C.

ISBN: 978-3-95450-234-9 ISSN: 2673-5504 doi:10.18429/JACoW-SRF2023-MOPMB041

GND Distributions in Nb Sheet After Heat Treatment

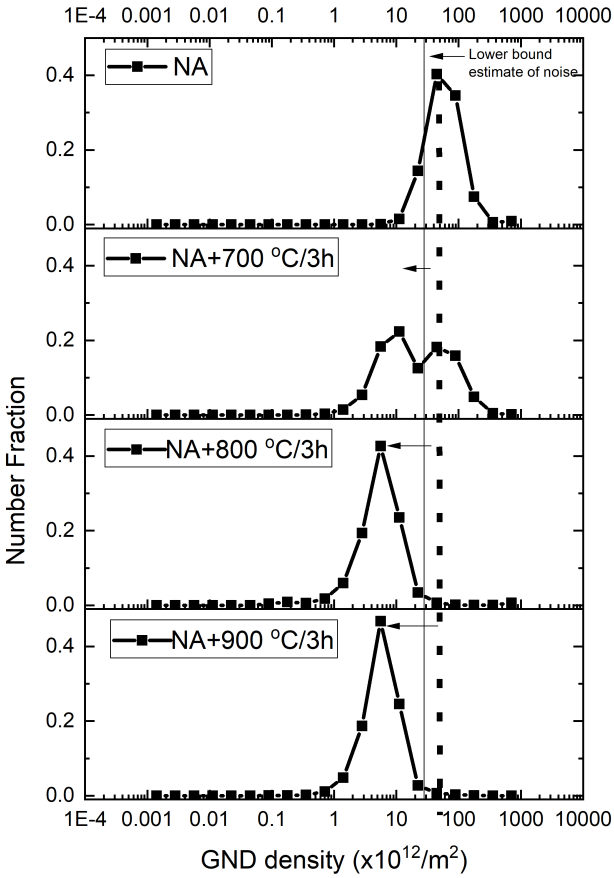

Figure 4: Evolution of the GND density with decreasing temperature shows a clear shift towards lower GND values as Nb transforms from the cold work state to the recrystallized after 800 °C/3 h, 900 °C/3 h treatments.

GND density for the four process conditions are plotted as a function of heat treatment temperature in Fig. 4. For the non-annealed sheet, the modal value of the GND peak is 22×10^{12}/m^2. With successive heat treatments, the dislocation density decreases, lowering the local misorientation gradients, and hence the GND distributions tend to shift to the left. After the 700 °C/3 h heat treatment, the GND distribution is bi-modal, with peaks at 11×10^{12}/m^2 and 45×10^{12}/m^2. From the OIM images in Fig. 2b and f, we know that the microstructure consists of recrystallized and cold-worked regions. The 45×10^{12}/m^2 peak value correlates well with the NA sample. Both 800 °C/3 h and 900 °C/3 h samples have a single peak with similar distributions at 6×10^{12}/m^2. We interpret this low number as a characteristic of recrystallization and grain growth. The recrystallization percent for the 700 °C is calculated for from the GND distributions using the ratios of areas under the bi-modal peaks indicates a recrystallization of 58%.

A low estimate noise floor ($\Delta\rho$) calculated, is dependent on the angular accuracy (δ), step size used for the EBSD scan (λ) , and the burgers vector (b), given by: $\Delta\rho = \delta/b\lambda$ [23]. For the present dataset the angular accuracy of EBSD, δ ($= 8\times10^{-3}$ rad), burgers vector, b(=0.2886 nm), and EBSD step size, λ (=1 µm). For the parameters used in this paper the noise estimate is 28 x 10^{12} /m^2, which is high and comparable with the GND values obtained in this dataset. Nevertheless, the GND peak is slightly sharper for the 900 °C sample compared with the peak for the 800 °C sample, suggesting that there could be the potential to quantify more subtle variations in microstructure using this technique.

DISCUSSION

The dataset presented here from the near-surface cross-sectional microstructure of the non-annealed cavity sheet after 800 °C, and 900 °C/3 h shows a high level of recrystallization. We would expect that the cavity formed using the non-annealed sheet and then annealed at 800 °C/3 h would also have a high level of recrystallization, which is consistent with the increased level of flux expulsion in the corresponding cavity compared to the one using traditional (annealed) sheet. However, the non-annealed sheet cavity even after 800 °C/3 h requires a high-temperature differential on cooling to expel flux, indicating that there still are flux pinning centers that are present in the microstructure that are reduced in quantity by the 900 °C HT as indicated by the cavity flux-expulsion tests.

Recent recrystallization experiments on 30% cold rolled Nb sheets indicate a strain path dependence on recrystallization [19]. An open question: How do strain path variations affect the recrystallization behavior after 800 °C/3 h? Do they have any detrimental influence on recrystallization and hence flux trapping? Figure 2c and g, show that refined grains are trapped between large grains after the 800 °C/3 h microstructure and at the surface after 900 °C/3 h. The fine grains at the surface have been observed during prior recrystallization studies of SRF-grade Nb wires where the GND densities are high [24]. With a step size of 1 µm, we could not discern any difference in GND density.

Our previous results indicate that flux expulsion is more demanding in these fine grain regions (~ 30 - 50 µm) than in larger grain regions (> 100 µm) [11]. A recent analysis of cavity results correlating starting grain size of the Nb sheet shows strong correlations between fine grain size and flux trapping [25]. The current work indicates that refined grains in the starting microstructure may also correlate to incomplete recrystallization, as observed after the 700 °C/3 h heat treatment, where the average grain size is about 50 µm. The vendor does not supply the percent cold work of the Nb sheet and is likely to vary from vendor to vendor and possibly from sheet to sheet, so it may be necessary to develop recrystallization-relevant specifications. In order to deliver the traditionally specified average grain size of 50 µm, a 700 °C/3 h anneal could be performed. However, the results in Fig. 2b, indicate that complete recrystallization is not possible on this sheet at 700 °C/3 h to deliver this grain size specification. The influence of these un-recrystallized

ISBN: 978-3-95450-234-9 ISSN: 2673-5504 doi:10.18429/JACoW-SRF2023-MOPMB041

regions may persist in the microstructure even after cavity-level deformation and annealing at 800 °C/3 h and higher. Furthermore, the level of deformation varies from the iris to the equator in formed half-cells.

GND analysis can distinguish recrystallized microstructure in the presence of remnant deformation as observed after 700 °C/3 h samples. The average IQ map for SRF Nb is a metric worth exploring since the material is single phase, and the main contrast of concern is the strain and GB-based contrast. However, both GND and IQ methods can be susceptible to sample preparation and beam conditions. Sample damage due to improper polishing will affect the IQ numbers, pattern quality, and hence the EBSD analysis [26]. Our preliminary data on the application of GND data to quantify the process of recrystallization in SRF shows a bi-modal distribution after the 700 °C/3 h HT in contrast to the uni-modal distributions in both the NA, and after 800 °C, 900 °C/3 h, confirming previous work that the GND data could be used to develop a systematic method to characterize SRF Nb at various degrees of recrystallization. Typically, GND analysis has been used for deformed microstructures [22, 23, 27], and analyzing recrystallization behavior in SRF Nb is under development.

CONCLUSION

Nb SRF cavities are traditionally formed out of annealed sheets. Starting with non-annealed and post-annealing at 800 °C/3 h consistently show better flux expulsion, which improves the quality factor. The results of this study indicate that an initially cold worked sheet after an 800 °C/3 h heat treatment has a high recrystallized volume which correlates to increased flux expulsion efficiency. Changing the deformation level in the initial sheets and annealing after cavity fabrication could be a pathway to enable consistently high flux expulsion in Nb cavities requiring high-quality factors. IQ and GND-based calculations are able to separate recrystallized versus non-recrystallized structures globally. Both these quantities are subject to variation depending on sample preparation. For any quantification, consistent sample preparation procedures would be necessary. In addition, quantifying GND values requires a careful understanding of signal over noise and the impact of EBSD parameters in the regime of recrystallization and grain growth.

ACKNOWLEDGEMENTS

The authors acknowledge useful discussions with Prof. Eric Taleff, and Thomas Bennett who are with the University of Texas at Austin.

REFERENCES

[1] H. Padamsee, "50 years of success for SRF accelerators-a review", *Supercond. Sci. Technol.*, vol. 30, p. 053003, 2017. doi:10.1088/1361-6668/aa6376

[2] S. Belomestnykh *et al.*, "Key directions for research and development of superconducting radio frequency cavities", in *Proc. Snowmass 2021*, 2022. doi:10.48550/arXiv.2204.01178

[3] A. Grassellino *et al.*, "Unprecedented quality factors at accelerating gradients up to 45 MVm^{-1} in niobium superconducting resonators via low temperature nitrogen infusion", *Supercond. Sci. Technol.*, vol. 30, p. 094004, 2017. doi:10.1088/1361-6668/aa7afe

[4] P. Dhakal, S. Chetri, S. Balachandran, P. J. Lee, and G. Ciovati, "Effect of low temperature baking in nitrogen on the performance of a niobium superconducting radio frequency cavity", *Phys. Rev. Accel. Beams*, vol. 21, p. 032001, Mar. 2018. doi:10.1103/PhysRevAccelBeams.21.032001

[5] E. M. Lechner, J. W. Angle, F. A. Stevie, M. J. Kelley, C. E. Reece, and A. D. Palczewski, "RF surface resistance tuning of superconducting niobium via thermal diffusion of native oxide", *Appl. Phys. Lett.*, vol. 119, no. 8, p. 082601, Aug. 2021. https://doi:10.1063/5.0059464

[6] G. Ciovati, "Improved oxygen diffusion model to explain the effect of low-temperature baking on high field losses in niobium superconducting cavities", *Appl. Phys. Lett.*, vol. 89, no. 2, p. 022507, Jul. 2006. doi:10.1063/1.2220059

[7] D. Bafia, A. Grassellino, and A. Romanenko, "The Role of Oxygen Concentration in Enabling High Gradients in Niobium SRF Cavities", Fermi National Accelerator Lab. (FNAL), Batavia, IL, USA, FERMILAB-CONF-21-320-TD, Jan. 2021. https://www.osti.gov/biblio/1832824

[8] S. Posen *et al.*, "Role of magnetic flux expulsion to reach $Q_0 > 3 \times 10^{10}$ in superconducting rf cryomodules", *Phys. Rev. Accel. Beams*, vol. 22, no. 3, p. 032001, Mar. 2019. doi:10.1103/PhysRevAccelBeams.22.032001

[9] P. Dhakal, G. Ciovati, and A. Gurevich, "Flux expulsion in niobium superconducting radio-frequency cavities of different purity and essential contributions to the flux sensitivity", *Phys. Rev. Accel. Beams*, vol. 23, p. 023102, 2020. doi:10.1103/PhysRevAccelBeams.23.023102

[10] C. Z. Antoine, "Influence of crystalline structure on rf dissipation in superconducting niobium", *Phys. Rev. Accel. Beams*, vol. 22, p. 034801, 2019. doi:10.1103/PhysRevAccelBeams.22.034801

[11] S. Balachandran *et al.*, "Direct evidence of microstructure dependence of magnetic flux trapping in niobium", *Sci. Rep.*, vol. 11, no. 1, Mar. 2021. doi:10.1038/s41598-021-84498-x

[12] D. Gonnella, J. Kaufman, and M. Liepe, "Impact of nitrogen doping of niobium superconducting cavities on the sensitivity of surface resistance to trapped magnetic flux", *J. Appl. Phys.*, vol. 119, p. 073904, 2016. doi:10.1063/1.4941944

[13] M. Martinello *et al.*, "Effect of interstitial impurities on the field dependent microwave surface resistance of niobium", *Appl. Phys. Lett.*, vol. 109, p. 062601, 2016. doi:10.1063/1.4960801

[14] D. Gonnella *et al.*, "Industrialization of the nitrogen-doping preparation for SRF cavities for LCLS-II", *Nucl. Instrum. Methods Phys. Res., Sect. A*,vol. 883, pp. 143–150. doi:10.1016/j.nima.2017.11.047

ISBN: 978-3-95450-234-9 ISSN: 2673-5504 doi:10.18429/JACoW-SRF2023-MOPMB041

[15] S. Posen *et al.*, "Efficient expulsion of magnetic flux in superconducting radiofrequency cavities for high Q applications", *J. Appl. Phys.*, vol. 119, p. 213903, 2016. doi:10.1063/1.4953087

[16] B. D. Khanal, S. Balachandran, S. Chetri, P. Dhakal, and P. J. Lee, "Magnetic Flux Expulsion in Superconducting Radio-Frequency Niobium Cavities Made from Cold Worked Niobium", in *Proc. NAPAC'22*, Albuquerque, NM, USA, Aug. 2022, pp. 611–614. doi:10.18429/JACoW-NAPAC2022-WEZE5

[17] T. R. Bieler *et al.*, "Physical and mechanical metallurgy of high purity Nb for accelerator cavities", *Phys. Rev. Spec. Top. Accel. Beams*, vol. 13, no. 3, p. 031002, Mar. 2010. doi:10.1103/PhysRevSTAB.13.031002

[18] D. Kang, T. R. Bieler, and C. Compton, "Effects of processing history on the evolution of surface damage layer and dislocation substructure in large grain niobium cavities", *Phys. Rev. Spec. Top. Accel. Beams*, vol. 18, no. 12, p. 123501, Dec. 2015. doi:10.1103/PhysRevSTAB.18.123501

[19] Z. L. Thune, C. McKinney, N. G. Fleming, and T. R. Bieler, "The Influence of Strain Path and Heat Treatment Variations on Recrystallization in Cold-Rolled High-Purity Niobium Polycrystals", *IEEE Trans. Appl. Supercond.*, vol. 33, no. 5, pp. 1–4, Aug. 2023. doi:10.1109/TASC.2023.3248533

[20] Z. L. Thune, N. Fleming, C. McKinney, E. M. Nicometo, T. R. Bieler, and S. Balachandran, "Ex-Situ Investigation of the Effects of Heating Rate on the Recrystallization in Rolled Polycrystals of High-Purity Niobium", in *Proc. SRF'21*, East Lansing, MI, USA, Jun.-Jul. 2021, pp. 1–5. doi:10.18429/JACoW-SRF2021-SUPCAV002

[21] D. P. Field, P. B. Trivedi, S. I. Wright, and M. Kumar, "Analysis of local orientation gradients in deformed single crystals", *Ultramicroscopy*, vol. 103, no. 1, pp. 33–39, Apr. 2005. doi:10.1016/j.ultramic.2004.11.016

[22] J. Jiang, T. B. Britton, and A. J. Wilkinson, "Measurement of geometrically necessary dislocation density with high resolution electron backscatter diffraction: Effects of detector binning and step size", *Ultramicroscopy*, vol. 125, pp. 1–9, Feb. 2013. doi:10.1016/j.ultramic.2012.11.003

[23] A. J. Wilkinson and D. Randman, "Determination of elastic strain fields and geometrically necessary dislocation distributions near nanoindents using electron back scatter diffraction", *Philos. Mag.*, vol. 90, no. 9, pp. 1159–1177, Mar. 2010. doi:10.1080/14786430903304145

[24] Z.-H. Sung, A. Dzyuba, P. J. Lee, D. C. Larbalestier, and L. D. Cooley, "Evidence of incomplete annealing at 800 °C and the effects of 120 °C baking on the crystal orientation and the surface superconducting properties of cold-worked and chemically polished Nb", *Supercond. Sci. Technol.*, vol. 28, no. 7, p. 075003, May 2015. doi:10.1088/0953-2048/28/7/075003

[25] Z. H. Sung, P. Kulyavtsev, M. Martinello, D. Gonnella, M. Ross, and S. Posen, "Evaluation of predictive correlation between flux expulsion and grain growth for superconducting radio frequency cavities", Mar. 2023. doi:10.48550/arXiv.2303.14122

[26] S. I. Wright and M. M. Nowell, "EBSD Image Quality Mapping", *Microsc. Microanal.*, vol. 12, no. 1, pp. 72–84, Feb. 2006. doi:10.1017/S1431927606060090

[27] C. Moussa, M. Bernacki, R. Besnard, and N. Bozzolo, "Statistical analysis of dislocations and dislocation boundaries from EBSD data", *Ultramicroscopy*, vol. 179, pp. 63–72, Aug. 2017. doi:10.1016/j.ultramic.2017.04.005